AERONET-OC: A Network for the Validation of Ocean Color Primary Products

GIUSEPPE ZIBORDI,* BRENT HOLBEN,+ ILYA SLUTSKER,# DAVID GILES,# DAVIDE D'ALIMONTE,@ FRÉDÉRIC MÉLIN,* JEAN-FRANÇOIS BERTHON,* DOUG VANDEMARK,& HUI FENG,& GREGORY SCHUSTER,** BRYAN E. FABBRI,** SEPPO KAITALA,++ AND JUKKA SEPPÄLÄ++

* *Global Environment Monitoring Unit, Joint Research Centre, Ispra, Italy*
\+ *NASA Goddard Space Flight Center, Greenbelt, Maryland*
\# *Science Systems and Applications, Inc., Goddard Space Flight Center, Greenbelt, Maryland*
@ *Centro de Inteligência Artificial, Universitade Nova de Lisbon, Caparica, Portugal*
& *OPAL, University of New Hampshire, Durham, New Hampshire*
** *NASA Langley Research Center, Hampton, Virginia*
++ *Finnish Environment Institute, Marine Centre, Helsinki, Finland*

(Manuscript received 10 July 2008, in final form 9 February 2009)

ABSTRACT

The ocean color component of the Aerosol Robotic Network (AERONET-OC) has been implemented to support long-term satellite ocean color investigations through cross-site consistent and accurate measurements collected by autonomous radiometer systems deployed on offshore fixed platforms. The AERONET-OC data products are the normalized water-leaving radiances determined at various center wavelengths in the visible and near-infrared spectral regions. These data complement atmospheric AERONET aerosol products, such as optical thickness, size distribution, single scattering albedo, and phase function. This work describes in detail this new AERONET component and its specific elements including measurement method, instrument calibration, processing scheme, quality assurance, uncertainties, data archive, and products accessibility. Additionally, the atmospheric and bio-optical features of the sites currently included in AERONET-OC are briefly summarized. After illustrating the application of AERONET-OC data to the validation of primary satellite products over a variety of complex coastal waters, recommendations are then provided for the identification of new deployment sites most suitable to support satellite ocean color missions.

1. Introduction

The Aerosol Robotic Network (AERONET) is a system of globally distributed autonomous sun photometers that was established in the early 1990s to support atmospheric studies at various scales through standardized measurements of the direct sun irradiance and sky radiance (Holben et al. 1998). AERONET has been instrumental to the investigation of aerosol optical properties, the creation of global aerosol climatology, and the validation of atmospheric remote sensing products. Since 2006, the network has been expanded through a new component called AERONET-Ocean Color (AERONET-OC), which provides the additional capability of determining the radiance emerging from the sea—from which the so-called normalized water-leaving radiance L_{WN} is derived—with modified sun photometers installed on offshore fixed platforms. The ultimate purpose of AERONET-OC is the production of standardized measurements that are performed at different sites with identical measuring systems and protocols, calibrated using a single reference source and method, and processed with the same code (Zibordi et al. 2006c).

The objective of the work is to provide a comprehensive overview of AERONET-OC by presenting its elements as well as an example of the application of data products. Emphasis is given to the applied quality-assurance methods, an analysis of uncertainties, and a brief outline of the current AERONET-OC sites along with general recommendations for new deployments.

Corresponding author address: Giuseppe Zibordi, Global Environment Monitoring Unit, Joint Research Centre, 21027 Ispra, Italy.
E-mail: giuseppe.zibordi@jrc.it

DOI: 10.1175/2009JTECHO654.1

© 2009 American Meteorological Society

2. Background

The normalized water-leaving radiance $L_{WN}(\lambda)$ at various center wavelengths λ in the visible and near-infrared spectral regions is the primary ocean color radiometric product. This is determined from top-of-atmosphere radiance measurements corrected for the perturbing effects of the atmosphere. Higher-level products, like chlorophyll *a* concentration or seawater inherent optical properties (e.g., absorption and scattering) are all derived from $L_{WN}(\lambda)$ through bio-optical algorithms. Therefore, the validation and merging of remote sensing products from different earth observation (EO) systems require accurate, frequent, globally distributed, and highly consistent in situ measurements of $L_{WN}(\lambda)$.

Recent developments in above-water radiometry (Mobley 1999; Hooker et al. 2002a; Zibordi et al. 2002) led to the development of a fully autonomous above-water radiometer system (Zibordi et al. 2004). This is based on the extended capability of CIMEL Electronique (Paris, France) CE-318 automated sun photometers to perform marine radiometric measurements for determining $L_{WN}(\lambda)$ in addition to the regular measurements for retrieving aerosol optical properties. This CIMEL-based system, called the Sea-Viewing Wide Field-of-View Sensor (SeaWiFS) Photometer Revision for Incident Surface Measurements (SeaPRISM), performs multiple sky- and sea-radiance measurements at given viewing and azimuth angles at eight (nine in the most recent instrument release) center wavelengths in the 412–1020-nm spectral range.

Following the deployment of the first operational SeaPRISM system on an oceanographic tower in the Adriatic Sea in May 2002, the outstanding agreement obtained between $L_{WN}(\lambda)$ data determined from this system and an assessed in-water radiometer (Zibordi et al. 2004) led to consolidate the idea of a network of above-water autonomous radiometers operated at sites encompassing distinct water types suitable for satellite ocean color validation activities in coastal regions. In particular, the objective to generate in situ datasets representative of various marine trophic regimes by relying on standardized measurements obtained with identical instruments, protocols, calibration facility, and processing code is considered to be a major advance with respect to past field methods. In fact, this solution is expected to lessen potential inconsistencies inherent to global datasets of in situ measurements so far obtained by grouping data from several independent providers (Werdell and Bailey 2005) intrinsically affected by uncertainties because of different field instruments, diverse sampling methods, a variety of calibration sources and protocols, and assorted processing schemes.

Relying on the existing AERONET infrastructure for data handling, the performance of a test network of a few SeaPRISM systems was initially evaluated over a four year period using various deployment platforms positioned in different coastal locations (Zibordi et al. 2006c). Overall results from this testing phase, in combination with specific validation studies, fully confirmed the potential of this network for supporting satellite ocean color validation activities (Zibordi et al. 2006a,b; Feng et al. 2008).

3. The network

AERONET (Holben et al. 1998) is a federated instrument network and data archive managed by the National Aeronautics and Space Administration (NASA) Goddard Space Flight Center (GSFC) in partnership with the Laboratoire d'Optique Atmosphérique (LOA) of the Université des Sciences et Technologies de Lille (France).

It was specifically conceived to support aerosol investigations at local, regional, and global scales through standardized instruments and methods (Holben et al. 2001). The network structure mostly relies on NASA's commitment for field instrument calibration, data processing, and archiving. These basic activities are complemented by independent globally distributed actions focused on establishing and maintaining CE-318 sun photometers at measurement sites of interest for individuals or institutions. This largely results in a partnership of principal investigators (PIs) contributing to the network with equipment and data and benefitting from AERONET's support services.

Key features of AERONET are (i) near-real-time data collection and processing (i.e., within a few hours); (ii) use of standardized instruments, calibration, and data processing; and (iii) open access to measurements and products through a specified data policy.

A strength of the AERONET program structure is its ability to support new or extended tasks, such as the handling of field instruments different than those commonly included in the network or the implementation of innovative algorithms for data analysis. This flexibility greatly aided the implementation of the AERONET-OC subnetwork.

a. The measurement system

The CE-318 autonomous sun photometer measures (i) the direct sun irradiance $E(\lambda, \theta_0, \phi_0)$ as a function of λ, sun zenith angle θ_0, and sun azimuth angle ϕ_0 for the retrieval of the atmospheric optical thickness and (ii) the sky radiance $L_i(\lambda, \theta', \phi)$ in a wide range of directions

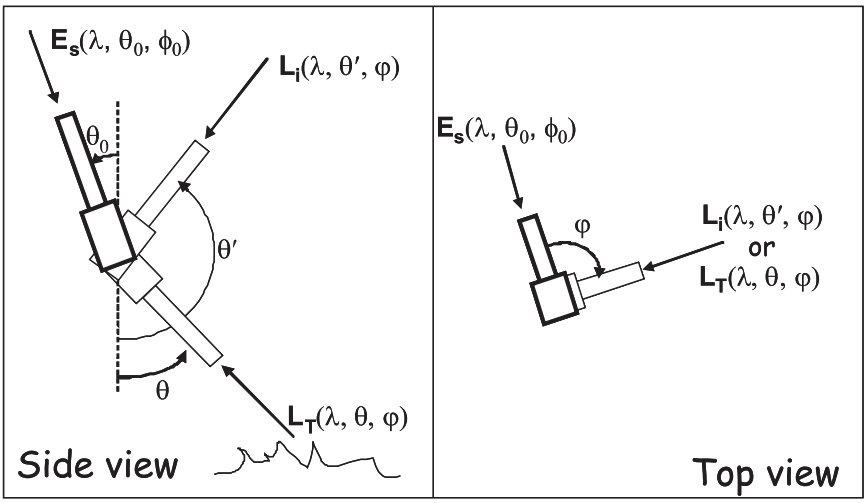

FIG. 1. SeaPRISM measurement geometry for $E_s(\lambda, \theta_0, \phi_0)$, $L_T(\lambda, \theta, \varphi)$, and $L_i(\lambda, \theta', \varphi)$.

identified by the viewing angle θ' and azimuth angle ϕ for the retrieval of the atmospheric scattering phase function. In addition to these atmospheric observations, SeaPRISM systems (i.e., CE-318 sun photometers modified to meet requirements for above-water radiometry) perform radiance measurements with a full-angle field of view of 1.2° to determine the total radiance from the sea $L_T(\lambda, \theta, \varphi)$ and the sky radiance $L_i(\lambda, \theta', \varphi)$ at relative azimuth angle with respect to the sun φ and with $\theta = \pi - \theta'$ (see Fig. 1). A feature of the system, which is useful for applications independent from AERONET-OC, is the possibility of changing some of the parameters that define the measurement sequence [i.e., θ and φ, the gain for each channel, and the numbers N_T and N_i of above-water and sky observations for determining $L_T(\lambda, \theta, \varphi)$ and $L_i(\lambda, \theta', \varphi)$, respectively].

The most recent SeaPRISM system configuration performs ocean color measurements at the 412-, 443-, 488-, 531-, 551-, and 667-nm center wavelengths. Additional measurements are performed at 870 and 1020 nm for quality checks, turbid water flagging, and the application of alternative above-water methods (Zibordi et al. 2002). These center wavelengths, as well as the wavelength at 940 nm, were selected to guarantee basic AERONET atmospheric aerosol and water vapor monitoring capabilities and to support essential validation activities for current ocean color EO systems.

In agreement with assessed measurement schemes, $L_T(\lambda, \theta, \varphi)$ and $L_i(\lambda, \theta', \varphi)$ values are determined at $\theta = 40°$ and $\varphi = 90°$. Larger φ values (e.g., $\varphi = 135°$; Mobley 1999), which are considered more appropriate than $\varphi = 90°$ for above-water observations, might lead to perturbations in radiometric measurements resulting from the deployment superstructure itself or its shadow. Details on the SeaPRISM sea-viewing measurement sequence were already given elsewhere (Zibordi et al. 2004). However, a summary is also provided here for the benefit of completeness.

Each SeaPRISM sea-viewing measurement sequence, which is executed every 30 min within ±4 h of 1200 LT, comprises the following:

(i) A series of direct sun measurements $E(\lambda, \theta_0, \phi_0)$ acquired at all channels for the determination of the aerosol optical thickness $\tau_a(\lambda)$, a quantity required for the determination of $L_{WN}(\lambda)$, and
(ii) A sequential set of N_T sea-radiance measurements for determining $L_T(\lambda, \theta, \varphi)$, and of N_i sky-radiance measurements for determining $L_i(\lambda, \theta', \varphi)$, serially repeated for each λ.

If the sun is cloud covered and consequently $E(\lambda, \theta_0, \phi_0)$ measurements are automatically stopped because of the low irradiance that is detected, then the whole measurement sequence is cancelled. The sky and sea measurements for determining $L_i(\lambda, \theta', \varphi)$ and $L_T(\lambda, \theta, \varphi)$ are performed with $N_i = 3$ and $N_T = 11$, respectively; the larger number of N_T measurements than N_i measurements is suggested by the higher environmental noise (mostly produced by wave perturbations) affecting the former measurements during clear sky.

b. Absolute calibration

Analogous to the basic CE-318 sun-photometers included in AERONET for ordinary aerosol applications, SeaPRISM systems are recalibrated every 6–12 months. Specific calibrations for measurements applied to determine $L_T(\lambda, \theta, \varphi)$ and $L_i(\lambda, \theta', \varphi)$ are carried out

either at the Joint Research Centre (JRC) or the GSFC. At the JRC, the calibration is made using 1000-W, quartz-halogen, tungsten coiled filament (FEL) lamps calibrated by Optronics Laboratories (Orlando, Florida) with an irradiance scale traceable to the National Institute for Standards and Technology (NIST) and an 18-in., 99%-reflectance Spectralon plaque from Labsphere, Inc. (North Sutton, New Hampshire) with 0°–45° directional–directional reflectance calibration. The expected uncertainty, including contributions from lamp iradiance, plaque reflectance, and mechanical setup, is 2.7% in the 400–1000-nm spectral interval as determined during the SeaWiFS Round Robin Experiment (SIRREX)-7 (Hooker et al. 2002b). The calibration at GSFC is performed using a 2-m integrating sphere (Walker et al. 1991) with an expected uncertainty lower than 5%. Comparison of calibration coefficients determined applying the two independent methods has shown maximum differences of 3% and spectrally averaged differences of 1.2% with a standard deviation of 1.1%. The SeaPRISM radiometric stability over time periods of approximately one year has shown values varying from 0.4% to 0.2% between 412 and 870 nm. These values have been computed as the median of variation coefficients from pre- and post-deployment calibration coefficients determined over nine independent deployments lasting 6–12 months each for two instruments contributing to AERONET-OC measurements from 2002 to 2007.

c. Data reduction

Data processing for the determination of $L_{\mathrm{WN}}(\lambda)$ is only applied to measurement sequences fulfilling the following criteria: (i) there is no missing value; (ii) dark values are below a given threshold; (iii) measurements are performed with ϕ_0 values included within site-dependent limits to minimize superstructure perturbations in $L_T(\lambda, \theta, \varphi)$; (iv) aerosol optical-thickness data have been determined; and (υ) wind speed is lower than 15 m s^{-1}.

For each measurement sequence qualified for the data processing, $L_i(\lambda, \theta', \varphi)$ is determined by simply averaging the N_i sky-radiance data. Differently, $L_T(\lambda, \theta, \varphi)$ is determined from the average of a fixed percent of the N_T sea-radiance measurements exhibiting the lowest radiance levels (i.e., 2 out of 11 in the case of SeaPRISM). This approach has been suggested by independent studies (Hooker et al. 2002a; Zibordi et al. 2002), which highlighted the need for an aggressive filtering of above-water measurements to minimize the perturbing effects of sea surface roughness in $L_T(\lambda, \theta, \varphi)$. An additional study (Hooker et al. 2004) has also shown that the filter performance does not appreciably vary by slightly increasing the full-angle field of view (e.g., from 1.5° to 3°).

From $L_T(\lambda, \theta, \varphi)$ and $L_i(\lambda, \theta', \varphi)$, the water-leaving radiance $L_W(\lambda, \theta, \varphi)$ (i.e., the radiance emerging from the sea quantified just above the sea surface) is computed as

$$L_W(\lambda, \theta, \phi) = L_T(\lambda, \theta, \phi) - \rho(\theta, \phi, \theta_0, W)L_i(\lambda, \theta', \phi), \tag{1}$$

where $\rho(\theta, \varphi, \theta_0, W)$ is the sea surface reflectance as a function of the measurement geometry identified by θ, φ, θ_0, and of the sea state expressed through wind speed W. The value of $\rho(\theta, \varphi, \theta_0, W)$ at a given θ and φ can be theoretically determined as a function of θ_0 and W (Mobley 1999).

The normalized water-leaving radiance $L_{\mathrm{WN}}(\lambda)$ is determined from $L_W(\lambda, \theta, \phi)$ as

$$L_{\mathrm{WN}}(\lambda) = L_W(\lambda, \theta, \phi)C_{\Re Q}(\lambda, \theta, \phi, \theta_0, \tau_a, \mathrm{IOP}, W) \times C_{f/Q}(\lambda, \theta_0, \tau_a, \mathrm{IOP})[D^2 t_d(\lambda)\cos\theta_0]^{-1}, \tag{2}$$

where the terms $C_{\Re Q}(\lambda, \theta, \phi, \theta_0, \tau_a, \mathrm{IOP}, W)$ and $C_{f/Q}(\lambda, \theta_0, \tau_a, \mathrm{IOP})$ are introduced to remove the dependence from the viewing geometry and the bidirectional effects in $L_W(\lambda, \theta, \phi)$, respectively:

$$C_{\Re Q}(\lambda, \theta, \phi, \theta_0, \tau_a, \mathrm{IOP}, W) = \frac{\Re_0}{\Re(\theta, W)}\frac{Q(\lambda, \theta, \phi, \theta_0, \tau_a, \mathrm{IOP})}{Q_n(\lambda, \theta_0, \tau_a, \mathrm{IOP})} \quad \text{and} \tag{3}$$

$$C_{f/Q}(\lambda, \theta_0, \tau_a, \mathrm{IOP}) = \frac{f_0(\lambda, \tau_a, \mathrm{IOP})}{Q_0(\lambda, \tau_a, \mathrm{IOP})}\left[\frac{f(\lambda, \theta_0, \tau_a, \mathrm{IOP})}{Q_n(\lambda, \theta_0, \tau_a, \mathrm{IOP})}\right]^{-1}. \tag{4}$$

The quantities $\Re(\theta, W)$ and $\Re_0$ [i.e., $\Re(\theta, W)$ at $\theta = 0$] account for sea surface reflectance and refraction, and they primarily depend on θ and W. The quantities $Q(\lambda, \theta, \varphi, \theta_0, \tau_a, \mathrm{IOP})$ and $Q_n(\lambda, \theta_0, \tau_a, \mathrm{IOP})$ are the so-called Q factors at viewing angle θ and at nadir (i.e., $\theta = 0$), respectively. The Q factor describes the anisotropic distribution of the in-water radiance field and mostly depends on θ, φ, θ_0, τ_a, and the seawater inherent optical properties (IOPs). The quantity $f(\lambda, \theta_0, \tau_a, \mathrm{IOP})$ is a function relating the apparent optical properties (and specifically the irradiance reflectance) to IOPs (Morel et al. 2002). It is recalled that, for optically complex coastal waters, the quantity f is generally replaced by f' (Loisel and Morel 2001). The quantities $f_0(\lambda, \tau_a, \mathrm{IOP})$ and $Q_0(\lambda, \tau_a, \mathrm{Chla})$ are the values of $f(\lambda, \theta_0, \tau_a, \mathrm{IOP})$ and $Q_n(\lambda, \theta_0, \tau_a, \mathrm{Chla})$ at $\theta_0 = 0$, respectively. The term

D^2 in (2) accounts for the variations in the Sun–Earth distance as a function of the day of the year, whereas the quantity $t_d(\lambda)$ is the atmospheric diffuse transmittance (Deschamps et al. 2004) computed utilizing $\tau_a(\lambda)$ determined from SeaPRISM measurements.

The values of $\Re(\theta, W)$, $Q(\lambda, \theta, \varphi, \theta_0, \tau_a, \mathrm{IOP})$, and $f(\lambda, \theta_0, \tau_a, \mathrm{IOP})/Q_n(\lambda, \theta_0, \tau_a, \mathrm{IOP})$ applied in (3) and (4) are determined from lookup tables produced for oceanic waters and from clear-sky conditions with aerosol optical thickness $\tau_a = 0.2$ at 550 nm, for various discrete λ, θ, φ, θ_0, and chlorophyll *a* concentration (Chla) expressing dependence on IOPs (Morel et al. 2002). Specifically, the center wavelengths included in the lookup tables are $\lambda = 412.5$, 442.5, 490, 510, 560, and 660 nm. Unlike an early implementation of the processing code (Zibordi et al. 2004), the Chla value is first assumed equal to 1 mg m^{-3} and successively estimated through an iterative procedure making use of regional band-ratio algorithms based on remote sensing reflectance $R_{\mathrm{rs}}(\lambda)$ (where $R_{\mathrm{rs}}(\lambda) = L_{\mathrm{WN}}(\lambda)/E_0(\lambda)$ with $E_0(\lambda)$ extra-atmospheric sun irradiance). The process, which requires successive recomputations of Eqs. (2)–(4), generally provides a convergence better than 0.1% on the Chla value at the first iteration. It is finally pointed out that, because of the current lack of lookup data at center wavelengths close to 870 and 1020 nm, the related measurements are processed assuming both $C_{\Re Q}(\lambda, \theta, \phi, \theta_0, \tau_a, \mathrm{IOP}, W)$ and $C_{f/Q}(\lambda, \theta_0, \tau_a, \mathrm{IOP})$ equal to 1.

Actual measurements of W, when available, are used for the data processing. Alternatively, data from National Centers for Environmental Prediction (NCEP) are applied.

The use of Chla to express the dependence of bidirectional effects on IOPs is mostly suitable for case 1 waters (i.e., chlorophyll-dominated waters). Nevertheless, it is applied to all AERONET-OC data because of the lack of an alternative consolidated correction scheme for case 2 waters (i.e., sediment- or yellow substance–dominated waters). Implications of the adoption of such a correction scheme are addressed in the uncertainty analysis (see section 3e).

d. Quality assurance

Analogously to regular AERONET atmospheric products, ocean color products are also classified at three different quality-assurance (QA) levels. Data at level 1.0 only include $L_{\mathrm{WN}}(\lambda)$ determined from complete measurement sequences satisfying the basic criteria addressed in section 3c. Level 1.5 L_{WN} data are derived from level 1.0 products for which (i) level 1.5 cloud screened aerosol optical-thickness data exist; (ii) a series of empirical thresholds are satisfied [i.e., $L_{\mathrm{WN}}(\lambda) > -0.01$ mW cm^{-2} μm^{-1} sr^{-1}, which indicates absence of exceedingly negative values at each λ; $L_{\mathrm{WN}}(412) < L_{\mathrm{WN}}(443)$, which is commonly expected in coastal waters; and $L_{\mathrm{WN}}(1020) < 0.1$ mW cm^{-2} μm^{-1} sr^{-1}, which suggests the absence of any reflecting obstacle along the optical path between the instrument and the water surface]; and (iii) the N_T sea-radiance measurements or N_i sky-radiance measurements exhibit low variance, which indicates low wave perturbations and no appreciable contamination by nonhomogeneous clouds, respectively. The latter quality test is quite effective in removing measurement sequences performed with high wind speed, which exhibit occasional high L_T values because of foam reflectance. Fully quality-assured level 2.0 data refer to $L_{\mathrm{WN}}(\lambda)$ determined from level 1.5 products for which (i) level 2 aerosol optical thickness data exist; (ii) pre- and postdeployment calibration coefficients for L_T and L_i measurements were determined and exhibit differences smaller than 5%; (iii) the $L_{\mathrm{WN}}(\lambda)$ spectral shapes are shown to be consistent through multiple tests based on statistical approaches (see following text); and (iv) the $L_{\mathrm{WN}}(\lambda)$ passing all former tests do not exhibit dubious values during a final spectrum-by-spectrum screening performed by an experienced scientist.

While most QA tests rely on the application of thresholds, the methodology applied for the assessment of the spectral consistency makes use of statistical methods effective in detecting artifacts in $L_{\mathrm{WN}}(\lambda)$ spectra normalized at 551 nm or the closest center wavelength (D'Alimonte and Zibordi 2006). In particular, the applied scheme rejects spectra exhibiting (i) low statistical representativeness within the dataset itself (self-consistency test); (ii) anomalous features with respect to a reference set of quality-assured data (relative-consistency test). The specific algorithms applied are (i) the auto-recursive Multilayer Perceptron Neural Network (MLP; Lerner et al. 1999) and K-Nearest Neighborhood (KNN; Bishop 1995) models, for assessing the self-consistency of the data and (ii) the Gaussian Mixture Model (GMM; Bishop 1995) for setting a novelty detection scheme (e.g., D'Alimonte et al. 2003) to assess the relative consistency of input spectra with respect to reference data (previously subjectively assessed). It is acknowledged that some valid spectra may be identified as inconsistent through this procedure. Because of this, the applied automated QA process is supported by an interactive analysis allowing for an analyst to visually check the individual spectra identified as inconsistent (see Fig. 2). This additional step allows for the rejection or acceptance of individual spectra on the basis of the judgment of an experienced scientist, and it further strengthens the confidence in QA products.

The current deployment sites (see Table 1) are the Acqua Alta Oceanographic Tower (AAOT) of the Italian

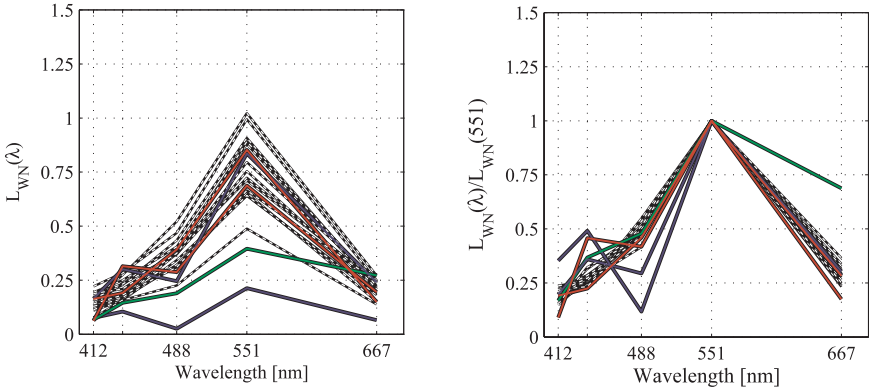

FIG. 2. Results from the spectral consistency analysis applied to a subset of L_{WN} data (mW cm^{-2} μm^{-1} sr^{-1}) determined from SeaPRISM measurements performed at the HLT site during 2007. (left) Absolute spectra and (right) spectra normalized with respect to the value determined at 555 nm. Inconsistent spectra are highlighted in different colors for different machine learning screening criteria. The red, green, and blue colors are used to identify inconsistent spectra detected through the MLP, KNN, and GMM tests, respectively. The black dashed lines indicate consistent spectra.

National Research Council (identified as Venice site within AERONET-OC), in the northern Adriatic Sea; the Gustaf Dalén Lighthouse Tower (GDLT) of the Swedish Maritime Administration, in the Baltic Sea; the Helsinki Lighthouse Tower (HLT) of the Finnish Maritime Administration, in the Gulf of Finland; the Martha's Vineyard Coastal Observatory (MVCO) tower of the Woods Hole Oceanographic Institution, in the Atlantic off the Massachusetts coast; the platform at the Clouds and the Earth's Radiant Energy System (CERES) Ocean Validation Experiment (COVE) site, in the Atlantic Ocean off the Virginia coast; and the Total Abu Al Bukhoosh oil platform (AABP), in the Persian Gulf. Results from the application of the QA tests to generate level 2 products are given in Table 2 for the current deployment sites.

Results in Table 2 indicate ranges of fully quality-assured data spanning from approximately 17% for AAOT down to 3% for AABP. These values depend on various factors, including deployment restrictions, cloudiness, environmental variability, instrument performance, and data transmission. For instance, note the 1.2% rejection rate for incomplete measurement sequences [i.e., incomplete data record or measurement sequence (IDR)] at COVE with respect to the GDLT and AABP values of 43%. That low rejection rate is explained by the alternative use of a caching computer for data collection instead of the common satellite data transmission, which may add communication errors. Also note the 0% data rejection at MVCO for azimuth limits [i.e., azimuth limits exceeded during the measurement sequence (ALE)] resulting from the peculiar superstructure utilized at the site, which offers a clear view of the sea at any possible daytime measurement geometry. In the case of AAOT, the high rejection of 35% of measurement sequences for azimuth limits is due to the stringent thresholds applied to avoid superstructure perturbations in sea-radiance observations. One of the most effective QA tests is that related to the aerosol optical thickness [i.e., missing τ_a values at level 2 (MAO)], which requires valid τ_a values for each sea-measurement sequence. Reasons for the removal of τ_a from the level 2 data, as well as for the consequent

TABLE 1. General information on the current AERONET-OC sites. The year in brackets indicates the first deployment. Height and depth refer to the height of the SeaPRISM deployment point and to the water depth (m), respectively, both with respect to the average sea level. Distance refers to the approximate distance from the mainland (n mi).

Site	Region	Lat	Lon	Height	Water depth	Distance	Structure
AAOT (2002)	Adriatic Sea	45.314°N	12.508°E	15	17	8	Oceanographic tower
GDLT (2005)	Baltic proper	58.594°N	17.467°E	26	16	9	Lighthouse
HLT (2006)	Gulf of Finland	59.949°N	24.926°E	30	13	12	Lighthouse
MVCO (2004)	U.S. Atlantic coast	41.325°N	70.567°W	12	15	2	Oceanographic tower
COVE (2005)	U.S. Atlantic coast	36.900°N	75.710°W	24	11	13	Lighthouse
AABP (2006)	Persian Gulf	25.495°N	53.146°E	24	23	80	Oil platform

TABLE 2. Statistics for the quality-assurance tests applied to upgrade data from raw to level 2. MS indicates the total number of measurement sequences on 31 Jan 2008 and QM indicates the number of final quality-assured measurements at level-2 (the related value in parentheses indicates the percent with respect to total). Values in columns indicate the percent of the total measurements sequences (i.e., MS) removed by each test. Symbols in the first row indicate the various exclusion tests applied: IDR; missing final calibration values (MCV); MAO; high dark values (HDV); ALE; high std dev in the N_T sea or N_i sky-radiance measurements (HSD); empirical threshold exceeded (ETE); SIC; and ISS (see text for acronym definitions).

	IDR	MCV	MAO*	HDV	ALE	HSD	ETE**	SIC	ISS
AAOT [MS = 24 328, QM = 4175 (17.1)]	15.8	2.9	23.1	1.0	35.0	3.4	1.1	0.3	0.1
GDLT [MS = 4932, QM = 427 (8.6)]	43.2	0.0	22.7	3.2	17.0	1.8	3.1	0.3	0.1
HLT [MS = 3372, QM = 374 (11.1)]	22.8	0.0	29.0	0.7	18.8	3.1	12.4	1.5	0.9
MVCO [MS = 6411, QM = 951 (14.8)]	17.2	4.4	53.9	0.0	0.0	4.6	4.9	0.2	0.1
COVE [MS = 3396, QM = 367 (10.8)]	1.2	1.1	42.2	0.0	23.6	4.6	20.8	1.4	0.4
AABP [MS = 7916, QM = 237 (3.0)]	43.1	19.8	11.9	1.0	11.4	4.0	4.4	1.1	0.3

* Test applied for invalid τ_a values at level 2.
** The exclusion thresholds are $W > 15\ \mathrm{m\,s^{-1}}$, $L_{\mathrm{WN}}(412) > L_{\mathrm{WN}}(443)$, $L_{\mathrm{WN}}(1012) > 0.1$, $L_{\mathrm{WN}}(\lambda) < -0.01$ [with L_{WN} (mW cm^{-2} μm^{-1} sr^{-1})].

exclusion of the corresponding L_{WN} spectra, are (i) possible cloud contamination detected during the quality assurance of aerosol products at level 1.5 (Holben et al. 2006; Smirnov et al. 2000) or (ii) large sensitivity changes occurring to the $E(\phi_0, \theta_0, \lambda)$ sensor during the deployment period and detected from the comparison of pre- and postdeployment calibration coefficients.

Finally, the effectiveness of the spectral-consistency test in detecting anomalous spectra is evident in Table 2. On average, this test identifies 3/4 of the overall anomalous spectra left in the database after the application of the major quality-assurance tests [see results from the inconsistency in L_{WN} spectra detected through statistical methods (SIC) test in Table 2]. The remaining dubious spectra removed through the subjective analysis by an experienced scientist, on average, are just a few tenths of a percent of the total number of measurements [see the values related to the spectra removed after individual analysis by experienced scientist (ISS) test in Table 2].

e. Uncertainties

The overall uncertainty of SeaPRISM $L_{\mathrm{WN}}(\lambda)$ data has been estimated by accounting for (i) absolute calibration uncertainty, (ii) changes in instrument sensitivity during each deployment period, (iii) uncertainty in corrections for the viewing-angle geometry and the anisotropy of the seawater light field, (iv) uncertainty in the determination of the $[D^2 t_d(\lambda)\cos\theta_0]^{-1}$ factor applied for the normalization of $L_W(\lambda)$, (v) uncertainty in the determination of the actual ρ, (vi) uncertainty in the actual value of W, and (vii) uncertainty because of environmental perturbations.

Estimates of individual uncertainties are specifically given in Table 3 for data produced at the AAOT, which exhibit the largest variability among L_{WN} derived at the various AERONET-OC sites. Uncertainties are only provided at the center wavelengths of major interest for ocean color applications: 412, 443, 488, 551 and 667 nm. Instead, the center wavelength at 531 nm has not been addressed because of limited data to date. Despite the importance of near-infrared L_{WN} data for the validation of atmospheric corrections, it was not possible to thoroughly quantify uncertainties at 870- and 1020-nm center wavelengths because they exhibit negligible L_{WN} values at all the current AERONET-OC sites.

Absolute calibration uncertainty is that assumed for radiance calibration performed at the JRC (see section 3b) and falling within the expected range of values (Hooker et al. 2002a). The uncertainty indicating the change in instrument sensitivity between successive calibrations has been determined from series of pre- and postdeployment calibration coefficients (see section 3b). Uncertainty in the factors applied to minimize effects

TABLE 3. Uncertainties of L_{WN} (percent) at various center wavelengths for measurements performed at the AAOT. Different terms indicate contributions from (i) uncertainties in absolute calibration; (ii) sensor sensitivity change between calibrations; (iii) uncertainty in the correction applied for removing dependences to the viewing angle and anisotropy of light field in seawater; (iv) uncertainty in the determination of t_d; (v) uncertainty in the determination of ρ because of wave effects and data filtering; (vi) uncertainty in the value of W; and (vii) uncertainties due to environmental effects.

Source	L_{WN}				
	412	443	488	551	667
Absolute calibration	2.7	2.7	2.7	2.7	2.7
Sensitivity change	0.4	0.2	0.2	0.2	0.2
Correction	1.6	2.0	2.8	2.9	1.9
t_d	1.5	1.5	1.5	1.5	1.5
ρ	1.8	1.3	0.7	0.6	2.5
W	1.1	0.8	0.4	0.4	0.4
Environmental effects	3.1	2.1	2.1	2.1	6.4
Quadrature sum	5.1	4.5	4.7	4.7	7.8

of viewing-angle geometry and anisotropy of the light distribution has been assumed equal to 25% of the median value of the applied $C_{\Re Q}(\lambda, \theta, \phi, \theta_0, \tau_a, \mathrm{IOP}, W) \times C_{f/Q}(\lambda, \theta_0, \tau_A, \mathrm{IOP})$ correction factor. This relatively large uncertainty has been defined on the basis of f/Q and f'/Q data determined from measurements performed at the AAOT site (Berthon and Zibordi 2004). These data, which are representative of a wide range of bio-optical conditions and show a low spectral dependence, exhibit a spectrally averaged value approximately (i) 20% higher than the average f/Q modeled by Morel et al. (2002) for oceanic waters (with Chla = 1.0 mg m^{-3} and $\theta_0 = 45°$); and (ii) 40% higher and 15% lower than the average f'/Q modeled by Loisel and Morel (2001) for yellow substance– and sediment-dominated waters, respectively.

The uncertainty in the determination of $[D^2 t_d(\lambda) \cos\theta_0]^{-1}$ has been empirically set to 1.5% at all center wavelengths. This value is expected to account for any approximation implicit in the relationship itself and for uncertainties in quantities required for the computation of t_d. For instance, it was found that the sole uncertainty of 0.02 assigned to τ_a (Holben et al. 1998) leads to an uncertainty of approximately 0.4% in $[D^2 t_d(\lambda)\cos\theta_0]^{-1}$ and consequently in L_{WN} at all center wavelengths [this uncertainty value was estimated as the median of the variation coefficients of L_{WN} determined for the entire AAOT dataset using $\tau_a(\lambda)$ and $\tau_a(\lambda) \pm 0.02$].

The determination of L_T using relative minima among the N_T measurements certainly leads to a reduction of glint-induced perturbations. However, a side effect of this filtering is an increased uncertainty in L_{WN} because of the determination of ρ and $\Re$ as a function of the actual value of W (which is used to parameterize the reflectance of the sea surface). In fact, the filtered L_T measurements relate to a sea surface that may no longer be statistically represented through the actual W.

In view of estimating the effects of the filtering process on L_{WN}, let us neglect changes in $\Re$ as a function of W with respect to the changes in ρ. This is fully justified for θ_0 in the range of 0°–70°, because variations of W from 0 to 15 m s^{-1} (i.e., the QA threshold) induce changes of several tens of percent in ρ (Mobley 1999) and less than 0.5% in $\Re$. Recalling that the applied filtering scheme was suggested by experimental studies indicating the need to account for $W > 0$ to improve the convergence of L_W determined from in-water and above-water measurements (Hooker et al. 2004; Zibordi et al. 2004), the current solution of determining ρ as a function of the actual W might thus lead to an underestimate of L_{WN}. On the contrary, it would lead to its overestimate with null values of W. Because of this, uncertainties in L_{WN} resulting from inconsistencies in the determination of ρ have been estimated as the median of variation coefficients of L_{WN} computed with null and actual values of W. These estimates exhibit uncertainty values varying from 1.8% to 0.6% between 412 and 551 nm and values of 2.5% at 667 nm.

The additional uncertainty possibly due to the lack of actual W has been determined as the median of percent differences between L_{WN} computed using values of W from NCEP and actual values from on-site hourly measurements, respectively. These uncertainties generally fall below 1%.

The effects of environmental perturbations—primarily due to wave effects and secondarily due to changes in the optical properties of seawater during the measurement sequence—are included in the uncertainty analysis. The specific uncertainty has been estimated as the median of variation coefficients for triplets of L_{WN} values determined from consecutive measurement sequences collected within approximately one hour. To minimize the impact of illumination changes in this estimate, the analysis has been restricted to data collected within ±2 h around 1200 LT. The computed values approximately vary within 2%–3% in the 412–551-nm interval and exhibit values above 6% at 667 nm. The higher values determined at 667 nm are mostly explained by the lower L_{WN} values determined in the red with respect to those at shorter center wavelengths. Slightly higher uncertainties resulting from environmental perturbations were presented elsewhere for L_W (Zibordi et al. 2004). Those values were assumed to include the effects of uncertainties in ρ and were quantified as the average of differences between two L_W values determined from successive measurement sequences rather than the median of variation coefficients for triplets of L_{WN} from consecutive measurement sequences.

The overall L_{WN} uncertainty budget, computed as the quadrature sum of the various individual sources assumed as independent, indicates values typically below 5% in the 412–551-nm spectral range and of approximately 8% at 667 nm, mostly because of environmental (sea surface) perturbations. With the exception of this last center wavelength in the red spectral interval, the uncertainties are within the target value of 5% defined for satellite ocean color missions (Mueller and Austin 1995) and certainly meet the 5% accuracy at around 443 nm indicated by Gordon and Clark (1981) for clear ocean waters. The relatively high uncertainty value estimated for L_{WN} at 667 nm indicates the difficulty of determining accurate L_{WN} in the red and near-infrared spectral regions. However, this limitation is also common to in-water radiometry.

Except for uncertainties on absolute calibration and sensitivity change, all the other uncertainties are tied to

TABLE 4. Values of marine and atmospheric optical properties for the various AERONET-OC sites: diffuse attenuation coefficient K_d (m^{-1}); absorption coefficient of yellow substance a_{ys} (m^{-1}) and coefficient defining its exponential spectral decrease S_y (nm^{-1}); Chla ($\mu g\ L^{-1}$); concentration of total suspended matter TSM ($mg\ L^{-1}$); aerosol optical thickness τ_a; and Ångström exponent α determined using τ_a at 490 and 870 nm.

Quantity	AAOT	GDLT	HLT	MVCO	COVE	AABP
K_d (490)	0.21 ± 0.09^a	0.34 ± 0.04^b	0.66 ± 0.09^b	0.18 ± 0.01^c	0.41 ± 0.26^d	—
a_{ys} (400)	0.20 ± 0.10^e	0.55 ± 0.10^b	0.89 ± 0.35^b	0.12 ± 0.01^f	0.17 ± 0.06^g	—
S_y (350–600)	0.017 ± 0.002^a	0.021 ± 0.001^b	0.022 ± 0.001^b	—	0.012 ± 0.002^g	—
Chla	1.3 ± 1.1^h	1.5 ± 0.4^b	3.0 ± 1.6^b	1.8 ± 1.0^c	4.4 ± 8.8^g	—
TSM	1.1 ± 0.7^h	1.0 ± 0.2^b	2.0 ± 0.7^b	1.5 ± 0.9^c	—	—
τ_a (412)	0.28 ± 0.22^i	0.15 ± 0.10^i	0.15 ± 0.10^i	0.19 ± 0.20^i	0.22 ± 0.26^i	0.42 ± 0.21^i
α (490–870)	1.57 ± 0.56^i	1.33 ± 0.36^i	1.36 ± 0.38^i	1.43 ± 0.46^i	1.20 ± 0.56^i	0.60 ± 0.43^i

[a] Data source: Zibordi and Berthon (2001).
[b] Data source: in situ data collected in the proximity of the two sites in August 2006 and August 2007.
[c] Data source: Subramaniam et al. (1999).
[d] Data source: Harding et al. (2005).
[e] Data source: Berthon et al. (2008).
[f] Data source: Sosik et al. (2001).
[g] Data source: Magnuson et al. (2004).
[h] Data source: Berthon et al. (2002).
[i] Data source: values determined from level 2 τ_a included in the AERONET-OC database on 31 Jan 2008.

average measurements performed at AAOT. It is then expected that the proposed typical uncertainty values might not equally apply to L_{WN} data from sites exhibiting L_{WN} variability different than that observed at AAOT.

f. Data handling and access

AERONET-OC makes full use of the existing AERONET data acquisition, processing, archiving, and distribution infrastructure managed by the NASA GSFC (Holben et al. 1998). Data acquisition mechanisms primarily include transmitters for relaying measurements to geostationary meteorological satellites [Geostationary Operational Environmental Satellite (GOES), Meteorological Satellite (Meteosat), or Geostationary Meteorological Satellite (GMS)] or the Internet for direct transfer of data to the AERONET system. The latter then processes SeaPRISM measurements in near–real time along with ancillary data input (e.g., NO_2, O_3, surface pressure, and W). Raw data and derived products at the various levels are stored in a specific database for each instrument on an hourly basis and are publicly available through the AERONET web interface (available online at http://aeronet.gsfc.nasa.gov) under specified data policies.

The AERONET Web site provides aerosol microphysical and optical property products (e.g., optical thickness, size distribution, phase function and single scattering albedo) together with L_{WN} data for each SeaPRISM site. Product map browsers provide a geospatial perspective of the available AERONET data for each site. Web interfaces provide site information, data plots, and support data download. Aerosol- and ocean color–derived products are displayed in daily, monthly, and yearly plots. Each data product may be browsed and downloaded by product type, date, and quality level. Additional related Earth science data products, such as atmospheric and oceanic satellite retrievals and 7-day back-trajectory analysis products, are also available for most AERONET sites. Furthermore, the AERONET Data Synergy Tool provides the supplementary capability to browse, analyze, and download multiple Earth science datasets through a single Web portal.

4. Atmospheric and marine features of current AERONET-OC sites

A basic requirement for operating a SeaPRISM system is its deployment on a fixed platform located in a marine (or lake) region at a distance from the mainland that minimizes the adjacency effects in satellite data. In addition, the water depth around the platform should be deep enough so that the bottom effects in L_{WN} are negligible. Accounting for these general criteria, platforms such as oceanographic towers, lighthouses, and derricks have been used to set up the current AERONET-OC sites (see Table 1). Relevant quantities describing seawater and atmospheric optical characteristics for each deployment region are summarized in Table 4. Further site details are presented through (i) SeaWiFS-derived maps of L_{WN} data to illustrate the general spatial features for each deployment region; (ii) 2D statistical representations of the level 2 L_{WN} AERONET-OC products, with the objective of showing

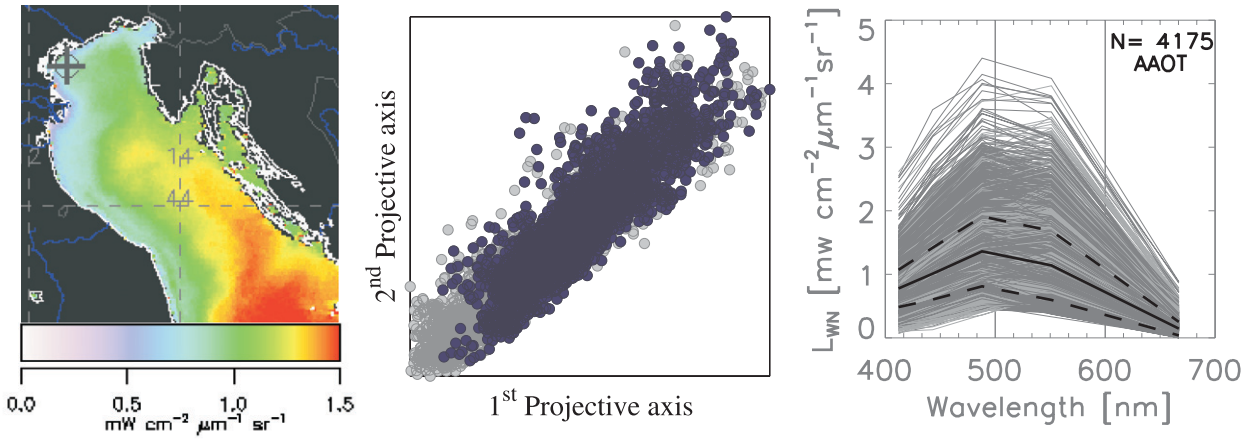

FIG. 3. (left) The 2003 summer composite (i.e., June–August) of SeaWiFS-derived $L_{WN}(443)$ maps for the AAOT area in the northern Adriatic Sea (the cross symbol indicates the AAOT site). (middle) A topographic representation of the distribution of the L_{WN} spectra in which each L_{WN} spectrum is projected on a single point in the 2D latent space by means of an autorecursive MLP. The data projection is based on L_{WN} data normalized with respect to their value at 551 nm (or at the closest center wavelength). Gray points represent the totality of spectra produced at the various AERONET-OC sites, whereas the blue points indicate spectra for the AAOT site. (right) Sample SeaPRISM $L_{WN}(\lambda)$ spectra for the AAOT site. The continuous thick line indicates averages, whereas thick dashed lines indicate values at ± 1 std dev with respect to averages.

differences among apparent optical properties across the various sites (see below); and (iii) level 2 L_{WN} AERONET-OC spectra, providing information on the site-specific seawater apparent optical properties.

The 2D representations of L_{WN} spectra normalized to 551 nm are provided through maps showing the distribution of data points corresponding to the site-specific spectral variability with respect to the totality of the level 2 spectra currently in the AERONET-OC database. These maps are displayed without axis scales because of the arbitrary rescaling of the input data during the mapping process by means of an auto-associative neural network scheme (D'Alimonte and Zibordi 2006). The similarity between normalized spectra presented in the same map is defined through the interpoint distance of their topographic projection, which means that similar L_{WN} spectral patterns correspond to points that are close in the map, whereas dissimilar spectral patterns correspond to points far from each other. The relevance of these maps relies on proposing a synoptic view of the overall AERONET-OC spectral shapes and thus highlighting their relative overall differences when utilized in bio-optical investigations through band ratios.

The AAOT site is frequently characterized by a large variability in bio-optical quantities because of its position in a transition region between open sea and coastal waters. This feature, illustrated in the left panel of Fig. 3, leads to data representing different water types with an occurrence of roughly 60% Case 1 water based on particulate matter only (Berthon et al. 2002; D'Alimonte et al. 2007). The topographic map in the middle panel of Fig. 3 shows that the apparent optical properties at the AAOT site exhibit similarity with those from MVCO, COVE, and AABP. The high variability shown by the AAOT L_{WN} spectra in the right panel of Fig. 3, provides a further confirmation of the wide range of bio-optical conditions occurring at this site. In agreement with independent radiometric measurements performed with in-water profilers, SeaPRISM L_{WN} spectra generally show maxima up to 4 mW cm^{-2} μm^{-1} sr^{-1} in the 490–555-nm spectral range because of absorption by yellow substance and a balance between pigmented and nonpigmented particles (Berthon et al. 2008).

The left panels in Figs. 4 and 5 suggest that both GDLT and HLT are located in relatively homogeneous areas (i.e., far from regions exhibiting large spatial gradients in bio-optical features). The topographic maps of L_{WN} data shown in the middle panels of Figs. 4 and 5 indicate differences in the apparent optical properties of the two sites and additionally astounding differences with respect to the AAOT L_{WN} data. These are clearly confirmed by the comparison of the L_{WN} spectra shown in the right panels of Figs. 4 and 5 with those in Fig. 3. The GDLT and HLT spectra exhibit very low absolute values, with minima at 412 and 667 nm and unique maxima at 551 nm below 1 mW cm^{-2} m^{-1} sr^{-1}. These spectra, characterized by a low variability, clearly confirm the presence of seawater dominated by yellow substance absorption. The spectrum appearing as an outlier and the few spectra exhibiting relatively high values at the blue–green center wavelengths in Fig. 4

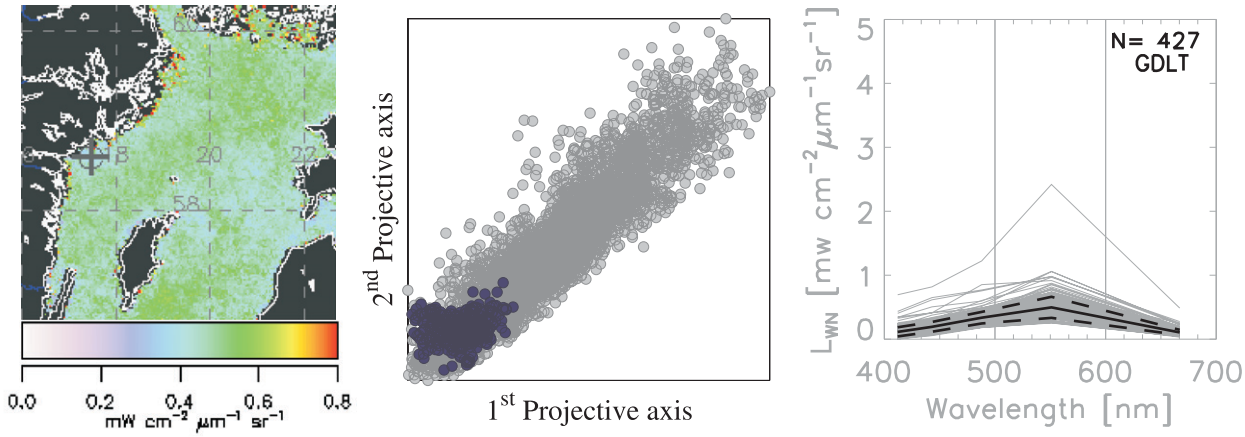

FIG. 4. As in Fig. 3, but for GDLT.

refer to measurements performed during a cyanobacterial bloom, which occurred in July 2005 over a large portion of the Baltic proper (Zibordi et al. 2006d).

Figure 6 (left panel) shows spatial gradients in L_{WN} near the MVCO site. As in the case of AAOT, this indicates the possibility of significant spatial variability in seawater bio-optical properties. The topographic map of L_{WN} data shown in the central panel indicates that the site-specific spectral characteristics are similar to those discernible at COVE (see section 4d) and, to some extent, AAOT. The L_{WN} spectra in the right panel display typical maxima at 551 nm, with values generally below 2.5 mW cm^{-2} μm^{-1} sr^{-1} and with shape and amplitude similar to those observed at COVE. These spectra confirm the presence of seawater moderately dominated by sediments.

Figure 7 (left panel) shows that COVE is also located near a transition region, which might be a source of large variability in the seawater bio-optical properties. As anticipated, the topographic map of L_{WN} data indicates the existence of spectral features almost equivalent to those detected at MVCO. Specifically, the L_{WN} spectra exhibit maxima at 551 nm with values generally below 2.5 mW cm^{-2} μm^{-1} sr^{-1}. Consistently with MVCO, these spectra also suggest the presence of seawater moderately dominated by sediments.

Figure 8 shows that the AABP is located in a relatively homogeneous area far from the heterogeneous bio-optical structures observable in front of the United Arab Emirates coast. The topographic maps of L_{WN} data displayed in the central panel indicate spectral features equivalent to some of those identified at the AAOT site. The L_{WN} spectra in the right panel indicate clear minima approaching zero at 667 nm and maxima at 488 nm with values generally below 1 mW cm^{-2} μm^{-1} sr^{-1}. These spectra, characterized by a relatively low variability in amplitude, suggest the presence of seawater dominated by chlorophyll *a*.

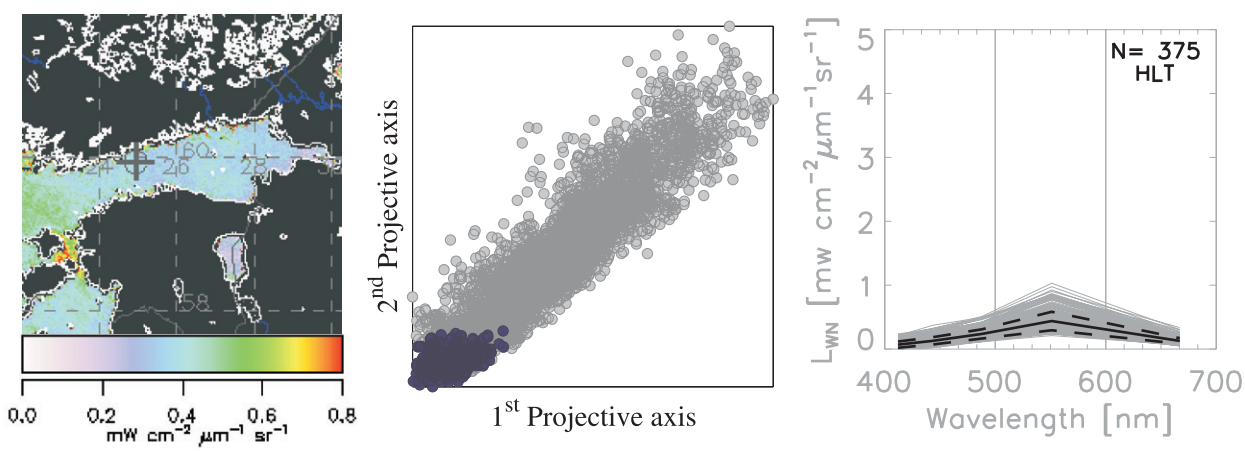

FIG. 5. As in Fig. 3, but for HLT.

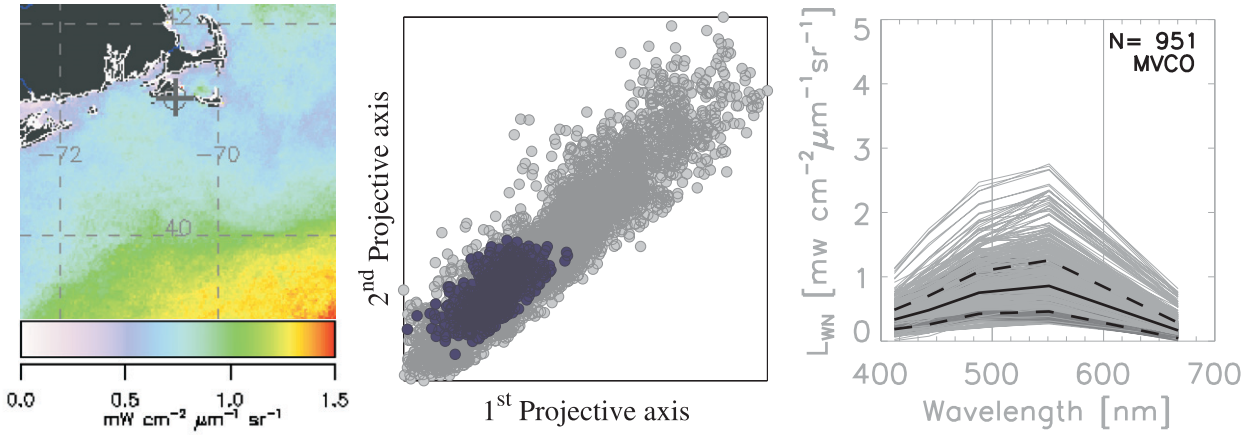

FIG. 6. As in Fig. 3, but for MVCO.

5. Applications

SeaPRISM data have shown a remarkable capability to support regional environmental investigations through radiometric time series measurements (Zibordi et al. 2006b,d; Feng et al. 2008). But even more exclusively, they have demonstrated their relevance for the assessment of the performance of ocean color EO systems in coastal waters. Remarkably, SeaPRISM data from the AAOT site contributed to point out the needs for improving MERIS data processing (Zibordi et al. 2006a), which later suggested revision of the atmospheric correction code and the possible implementation of a vicarious calibration scheme.

Table 5 provides statistics on the number of successful matchups (quasi-coincident satellite and in situ data) produced for different EO systems using AERONET-OC data at the AAOT site, for which a large number of SeaPRISM measurements exists. EO and in situ data taken within ±1 h, have been considered qualified for matchups when none of the 3 × 3 pixels centered at the AERONET-OC site is affected by the standard flags of the processing code (Bailey and Werdell 2006) mainly indicating cloud or sun-glint contaminations, an excessive viewing angle ($\theta > 60°$) or sun zenith angle ($\theta_0 > 70°$). Results indicate the capability of producing matchups at AAOT for more than 10% of the accessible ocean color EO products. This can be considered the target value for most of the AERONET-OC sites. A sensitivity analysis on matchup construction as a function of time and spatial variability utilizing AERONET-OC data is presented elsewhere (Zibordi et al. 2009).

Aiming at illustrating the potential of AERONET-OC in assessing primary EO products over different coastal regions characterized by specific optical properties, random samples from the global AERONET-OC dataset are applied to validate Moderate Resolution Imaging Spectroradiometer (MODIS) $L_{WN}(\lambda)$ and

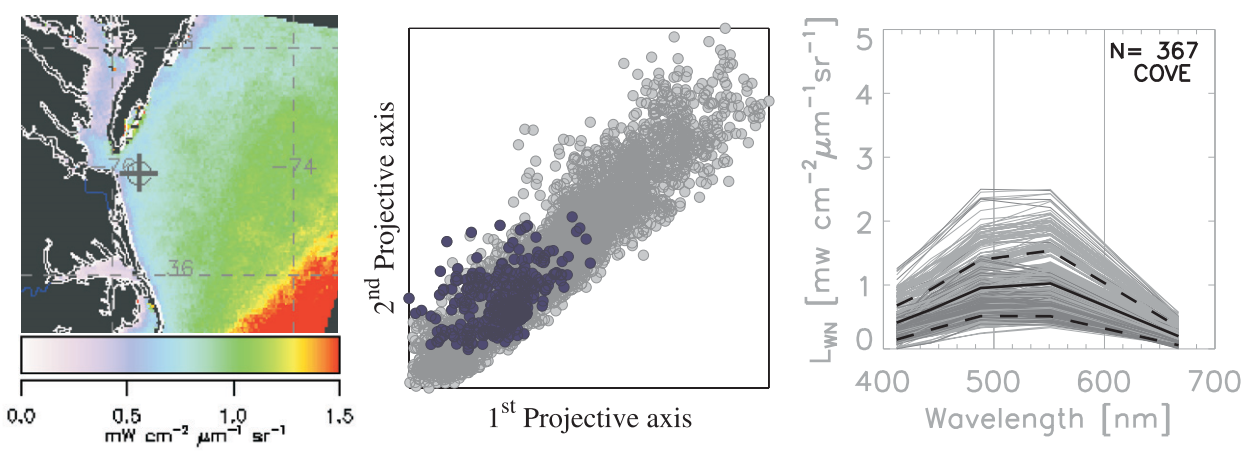

FIG. 7. As in Fig. 3, but for COVE.

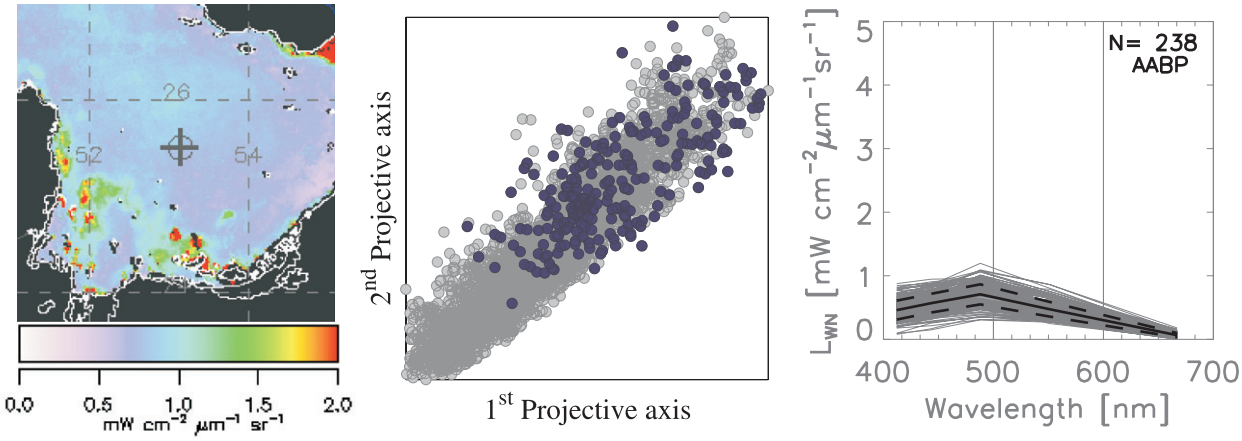

FIG. 8. As in Fig. 3, but for AABP.

$\tau_a(870)$ products. MODIS data for the comparison were generated using the SeaWiFS Data Analysis System (SeaDAS) software package (Fu et al. 1998) version 5.1.5 and screened as described in the previous paragraph. To minimize the impact of any differences in MODIS and SeaPRISM center wavelengths, a band-shift correction was applied to SeaPRISM L_{WN} data in agreement with the scheme illustrated by Zibordi et al. (2006a). Results from this exercise are presented in Fig. 9 and summarized through (i) the average of relative (signed) percent differences ψ between remote sensing and in situ data (to indicate the data bias) and (ii) the average of absolute (unsigned) percent differences $|\psi|$ (to indicate typical uncertainties).

The average differences between MODIS and SeaPRISM L_{WN} data are in general agreement with independent results presented for open sea regions (Franz et al. 2005; Bailey and Werdell 2006). The largest differences in terms of bias and scatter are observed at the 412- and 443-nm center wavelengths. This can be mostly explained by errors introduced in the atmospheric correction of EO data and partially traceable to the marine atmospheric optical characteristics of the sites and to the measurement geometry (D'Alimonte et al. 2008). Results obtained for τ_a are also in agreement with independent regional studies (Mélin et al. 2007b). In this case, residual differences can be attributed to (i) limits of the atmospheric correction scheme over regions that are characterized by complex coastal waters and influenced by continental aerosols and (ii) the lack of any vicarious calibration adjustment at $\lambda = 870$ nm.

6. Discussion

AERONET-OC relies on above-water radiometric data gathered with a system specifically developed for atmospheric measurements (i.e., for direct-sun-irradiance and sky-radiance measurements). This and unresolved issues such as the correction for the viewing angle and in-water nonisotropy effects from measurements performed in optically complex coastal waters, are sources of uncertainty at the 4%–5% level for L_{WN} data in the blue–green spectral regions. A reduction of these uncertainties requires more investigations and perhaps a radiometer redesign. Specific limitations, which could affect the uncertainty of data at the various sites as a function of the local seawater and atmospheric features, are addressed in the following subsections together with an overview of the requirements for new deployments.

a. Limitations

A major factor bounding the uncertainties of AERONET-OC data products is the CE-318 measurement technology. In fact, this system was mostly designed to sequentially measure, at a few center wavelengths, the sky radiance or the sun irradiance during stable illumination conditions (i.e., in the absence of cloud perturbations). This measurement technology shows two

TABLE 5. Total number of MERIS, MODIS, and SeaWiFS EO images available for the AAOT site for April 2002–September 2007. Qualified images and matchups indicate the number of EO images quality assured for matchup analysis and the actual number of matchups produced with the available SeaPRISM L_{WN} data (i.e., 4175 fully quality-assured spectra) for the considered period, respectively. Values in parentheses indicate percent values.

EO sensor	MERIS	MODIS	SeaWiFS
Total images	1022	2365	2889
Qualified images	302 (29.6)	505 (21.4)	580 (20.1)
Matchups	132 (12.9)	370 (15.7)	404 (14.0)

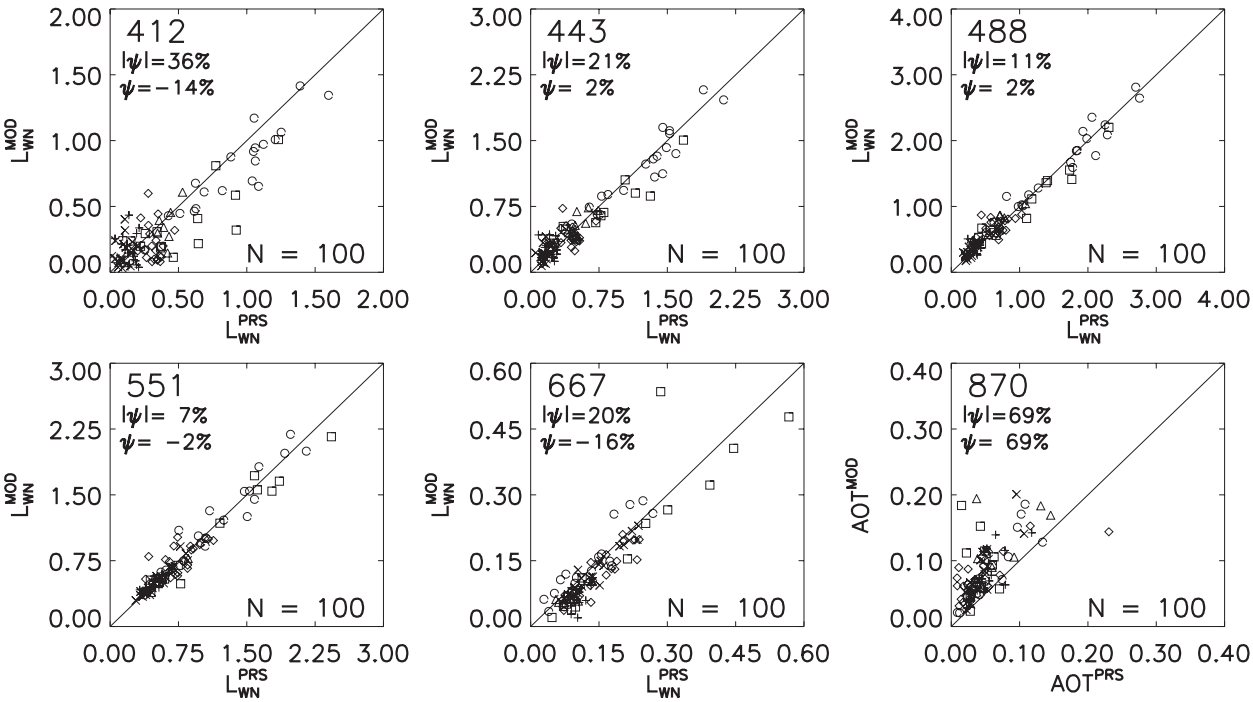

FIG. 9. Scatterplot of MODIS $L_{\mathrm{WN}}^{\mathrm{MOD}}$ vs SeaPRISM $L_{\mathrm{WN}}^{\mathrm{PRS}}$ data at various center wavelengths (i.e., 412, 443, 488, 551, and 667 nm) and scatterplot of MODIS vs SeaPRISM τ_a (i.e., AOT) at 870 nm, for 100 matchups realized from a subset of the current AERONET-OC data. Data points are indicated with a circle for AAOT (20 matchups), a plus for GDLT (20 matchups), a cross for HLT (20 matchups), a diamond for MVCO (20 matchups), a square for COVE (13 matchups), and a triangle for AABP (7 matchups). Symbol ψ indicates the average of relative (signed) percent differences between remote sensing and in situ data, whereas $|\psi|$ indicates the average of absolute (unsigned) percent differences.

major limitations in the case of sea-radiance observations. First, the collection of successive measurements at different time for different center-wavelengths increases the noise of $L_{\mathrm{WN}}(\lambda)$ spectra with respect to the case of measurements performed at the same time at all center wavelengths. Additionally, the limited number of spectral channels cannot support the production of data at center wavelengths and bandwidths exactly matching those of each ocean color EO system.

Although these limitations need to be accounted for when planning applications for AERONET-OC data products, their effects can be efficiently minimized. For instance, it is fully recognized that the time independence of measurements at the different center wavelengths and the random effects of wave perturbations will always lead to interband uncertainties in $L_{\mathrm{WN}}(\lambda)$ that are higher than those solely from absolute calibration. However, relative consistency tests based on quality-assured reference data can support the detection and removal of very noisy spectra. In addition, data collected at a few fixed center wavelengths can be optimally exploited by applying band-shift corrections based on regional bio-optical algorithms (Zibordi et al. 2006a; Mélin et al. 2007a; Zibordi et al. 2009).

A further methodological limitation currently affecting the processing of SeaPRISM data is the lack of operational tables for the determination of $C_{\Re Q}(\lambda, \theta, \phi, \theta_0, \tau_a, \mathrm{IOP}, W)$ and $C_{f/Q}(\lambda, \theta_0, \tau_A, \mathrm{IOP})$ at 870 and 1020 nm and more in general, tables applicable to optically complex coastal waters at any center wavelength. Given that specific studies of these aspects are ongoing (Park and Ruddick 2005), the exploitation of new research results in the AERONET-OC operational processing procedure should lead to future improvements of L_{WN} products.

b. *Network expansion deployment requirements*

Results from this first phase of AERONET-OC already confirms that SeaPRISM data products are a major complement to ship and mooring measurements for the assessment and merging of ocean color radiometric products. Additionally, in agreement with accuracy requirements for the Global Earth Observation System of Systems (GEOSS), AERONET-OC strengthens the capability to trace uncertainties in products from different EO systems by providing a time series of highly consistent in situ data collected at coastal sites exhibiting different marine bio-optical properties. These elements now call for an expansion of AERONET-OC

with additional and globally distributed measurement sites. General guidelines are thus provided to help identify new sites satisfying the SeaPRISM measurement requirements for ocean color applications.

The accurate sun tracking required for SeaPRISM measurements imposes that the deployment platform is a grounded structure. Deployment positions on any grounded structure with height- and shape-minimizing sea-spray contamination of the measuring unit allow for unobstructed sea observations at the maximum possible distance from the superstructure at the time of overpass of ocean color EO systems. Optimum deployment positions are hence in the uppermost western part of superstructures. Recalling that the minimization of superstructure perturbations in above-water radiometric measurements requires observations of the sea surface at distances at least equal to the superstructure height (Hooker and Zibordi 2005), it is suggested that SeaPRISM systems are deployed through dedicated platforms extending a few meters outside the main structure but still permitting system maintenance and sun-tracker alignment.

Any SeaPRISM deployment structure should ideally be at a distance from the mainland suitable to assume that the adjacency effects are negligible in EO data. The adjacency effects (Santer and Schmechtig 2000) are produced by a difference in the reflectance of adjacent surfaces, and the magnitude of the related perturbations in EO data are a function of the spectral reflectance of surfaces and of the optical properties of the atmosphere (i.e., the aerosol type and load). As a rule of thumb, any distance greater than 5–10 nautical miles is considered suitable. However, provided that the adjacency effects are accounted for, sites at close distance from the mainland (i.e., less than 5 nautical miles) are still relevant for the validation of EO products. Figure 10 shows the percent overestimate of the sea surface albedo derived from space at nadir view. Values are presented as a function of the distance from the coast and have been determined through a parametric relationship (Sei 2007) assuming a continental aerosol and two half-Lambertian surfaces (i.e., land and sea) with different spectral albedos. The applied parameterization includes the determination of the spectral aerosol optical thickness through $\tau_a = 0.05\lambda^{-1.6}$ (with λ in units of μm) and the choice of albedos 0.08, 0.06, and 0.25 at 551, 667, and 870 nm, respectively, for a cropland–urban ecosystem (Moody et al. 2005), and of 0.04, 0.03, and 0.025 at 551, 667, and 870 nm, respectively, for the sea with $\theta_0 = 30°$ (Jin et al. 2002). Adjacency effects are instead assumed negligible in the blue spectral region because of the closeness of sea and land albedos. Results indicate that, for the considered conditions, the absolute sea surface albedo from space at approximately 5 nautical miles from the coast is overestimated by 4%–5% at 667 and 551 nm and by more than 20% at 870 nm. At 10 nautical miles from the coast, the overestimate falls below 2% at 551 and 667 nm and 10% at 870 nm. However, a specific analysis of adjacency effects performed for AAOT, GDLT, and HLT, with synthetic transects of SeaWiFS-derived $\tau_a(865)$ and $L_{WN}(670)$ climatological data, indicate that the former theoretical results are probably appreciably overestimated (Zibordi et al. 2009).

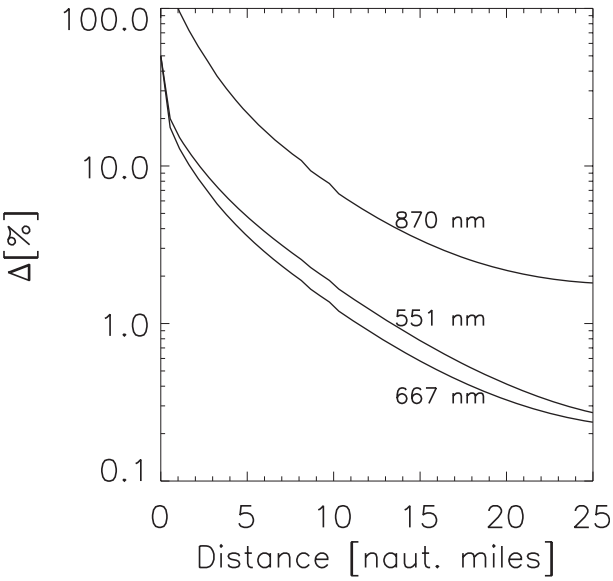

FIG. 10. Curves quantifying the percent variation in sea surface albedo (Δ) as a function of the distance from the coast for satellite nadir view at 551, 667, and 870 nm.

A further requirement for any ideal AERONET-OC site is that the water depth in the proximity of the deployment structure allows for neglecting the bottom effects. In this case the curves provided in Fig. 11 indicate, as a function of the seawater diffuse attenuation coefficient K_d and irradiance reflectance R, the water depth at which SeaPRISM L_{WN} measurements are increased by 1% by bottom perturbations resulting from a Lambertian seabed with irradiance reflectance $R_b = 0.10$. These curves were determined by adapting the equation proposed by Maritorena et al. (1994) to SeaPRISM sea-viewing observations (i.e., accounting for the in-water optical path related to L_T measurements) to quantify the bottom effects in subsurface reflectance data. According to data in Fig. 11, a deployment site satisfies the condition of negligible bottom perturbations if the water depth is larger than that identified by the values of R and K_d at the center wavelength exhibiting the deepest light penetration (in coastal waters, it generally falls in the 488–551-nm spectral range).

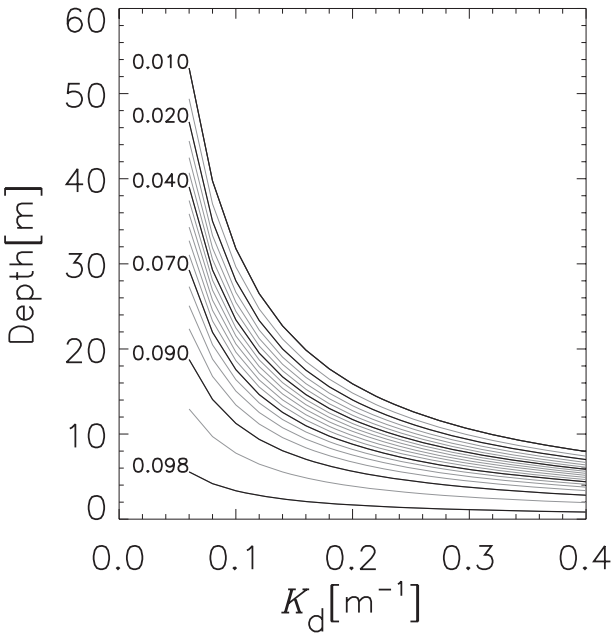

FIG. 11. Curves indicating the water depth at which the bottom perturbation adds a contribution of 1% to the SeaPRISM L_{WN}, as a function of seawater diffuse attenuation coefficient K_d, and irradiance reflectance R at any fixed λ (the latter values are given in the inner part of the panel for the curves in black), assuming a Lambertian seabed irradiance reflectance $R_B = 0.10$ (portion of some curves, whose values have been computed by independently varying K_d and R, might not represent realistic cases).

7. Summary

AERONET-OC aims to contribute to improved satellite ocean color applications through standardized measurements performed using autonomous radiometers operated on fixed platforms at coastal sites. This general objective was confirmed through the validation of satellite ocean color primary products (i.e., L_{WN} and τ_a), using autonomous systems deployed at sites characterized by very different atmospheric and seawater types.

An estimate of the overall uncertainty budget in AERONET-OC L_{WN} has shown values typically below 5% at the blue and green center wavelengths. Uncertainties of approximately 8% have been estimated for the red center wavelengths.

The quality assurance scheme applied to data from the current AERONET-OC sites has shown success rates ranging from 5% to 17% of the total measurements, depending on a wide range of causes including deployment restrictions, instrument misperformance, data transmission errors, and environmental factors such as cloudiness or wave perturbations.

Browsing, displaying, and downloading raw data and derived products is possible through the AERONET Web interface under a specified data policy. Additional Earth science data products such as atmospheric and oceanic satellite retrievals and 7-day back-trajectory analysis products are also accessible through the same Web interface for most of the sites.

The limits of the autonomous system and of the methodology used for the determination of AERONET-OC L_{WN} products have been discussed to inform data users, as well as to highlight research areas where future investigations might help reduce current uncertainties. Within this latter context, a major need is the development of operational tables to determine the correction factors for viewing angle and seawater nonisotropy effects for measurements performed in complex coastal waters.

Finally, deployment requirements have been delineated to facilitate the identification of new AERONET-OC sites. Specifically, suitable sites must rely on fixed deployment structures located in regions preferably satisfying the assumption of negligible adjacency effects in satellite-derived L_{WN} and negligible bottom perturbations.

Acknowledgments. The authors wish to thank Michel Grepinet of Total, Abu Al Bukhoosh for hosting the SeaPRISM at AABP, and Abdulla Al Mandoos, director of the Department of Atmospheric Studies, for providing maintenance for this site; the personnel of the AAOT site for the continuous support; Janet Fredricks, Heidi Sosik, Ru Morrison, Andy Girard, and Rob Olsen from the University of New Hampshire for their continued contributions at the MVCO site; Georgios Lampadaris from the Swedish Maritime Administration and Niklas Strömbeck from Strömbeck Consulting for their support in setting up and maintaining the GDLT site; and Marius Canini from CIMEL for the successive revisions of SeaPRISM firmware. Finally, the authors wish to thank the entire AERONET team for the efforts to include the ocean color component in the AERONET observational network.

REFERENCES

Bailey, S. W., and P. J. Werdell, 2006: A multi-sensor approach for the on-orbit validation of oceancolor satellite data products. *Remote Sens. Environ.,* **102,** 12–23.

Berthon, J. F., and G. Zibordi, 2004: Observed relationships between apparent and inherent optical properties in the northern Adriatic Sea. *Proc. Ocean Optics XVII Conf.,* Fremantle, Australia, The Oceanography Society, 7 pp.

——, ——, J. P. Doyle, S. Grossi, D. van der Linde, and C. Targa, 2002: Coastal Atmosphere and Sea Time Series (CoASTS), Part 2: Data analysis. NASA Tech. Memo. TM-2002-206892, Vol. 20, S. B. Hooker and E. R. Firestone, Eds., NASA Goddard Space Flight Center, 25 pp.

——, F. Mélin, and G. Zibordi, 2008: Ocean colour remote sensing of the optically complex European seas. *Remote Sensing of the European Seas,* V. Barale and M. Gade, Eds., Springer, 35–52.

Bishop, C. M., 1995: *Neural Networks for Pattern Recognition*. Oxford University Press, 504 pp.

D'Alimonte, D., and G. Zibordi, 2006: Statistical assessment of radiometric measurements from autonomous systems. *IEEE Trans. Geosci. Remote Sens.,* **44,** 719–728.

——, F. Mélin, G. Zibordi, and J.-F. Berthon, 2003: Use of the novelty detection technique to identify the range of applicability of empirical ocean colour algorithms. *IEEE Trans. Geosci. Remote Sens.,* **41,** 2833–2843.

——, G. Zibordi, and J.-F. Berthon, 2007: A statistical index of bio-optical seawater types. *IEEE Trans. Geosci. Remote Sens.,* **45,** 2644–2651.

——, ——, and F. Mélin, 2008: A statistical method for generating cross-mission consistent normalized water-leaving radiances. *IEEE Trans. Geosci. Remote Sens.,* **46,** 4075–4093.

Deschamps, P.-Y., B. Fougnie, R. Frouin, P. Lecomte, and C. Verwaerde, 2004: SIMBAD: A field radiometer for satellite ocean-color validation. *Appl. Opt.,* **43,** 4055–4069.

Feng, H., D. Vandemark, J. W. Campbell, and B. N. Holben, 2008: Evaluation of MODIS ocean colour products at a northeast United States coast site near the Martha's Vineyard coastal observatory. *Int. J. Remote Sens.,* **29,** 4479–4497.

Franz, B. A., and Coauthors, 2005: The continuity of ocean color measurements from SeaWiFS to MODIS. *Earth Observing Systems X,* J. J. Butler, Ed., International Society for Optical Engineering (SPIE Proceedings, Vol. 5882), 58820W, doi:10.1117/12.620069.

Fu, G., K. Baith, and C. McClain, 1998: The SeaWiFS data analysis system. *Proc. Fourth Pacific Ocean Remote Sensing Conf.,* Quigdao, China, 73–79.

Gordon, H. R., and D. K. Clark, 1981: Clear water radiances for atmospheric correction of Coastal Zone Color Scanner imagery. *Appl. Opt.,* **20,** 4175–4180.

Harding, L. W., D. Degobbis, and R. Precali, 1999: Production and fate of phytoplankton: Annual cycles and interannual variability. *Ecosystems at the Land-Sea Margin: Drainage Basin to Coastal Sea,* T. C. Malone et al., Eds., Vol. 55, *Coastal and Estuarine Studies,* Amer. Geophys. Union, 131–172.

Holben, B. N., and Coauthors, 1998: AERONET—A federated instrument network and data archive for aerosol characterization. *Remote Sens. Environ.,* **66,** 1–16.

——, and Coauthors, 2001: An emerging ground-based aerosol climatology: Aerosol optical depth from AERONET. *J. Geophys. Res.,* **106,** 12 067–12 097.

——, T. F. Eck, I. Slutsker, A. Smirnov, A. Sinyuk, J. Schafer, D. Giles, and O. Dubovik, 2006: AERONET's Version 2.0 quality assurance criteria. *Remote Sensing of Atmosphere and Clouds,* S. C. Tsay et al., Eds., International Society for Optical Engineering (SPIE Proceedings, Vol. 6408), 64080Q, doi:10.1117/12.706524.

Hooker, S. B., and G. Zibordi, 2005: Platform perturbation in above-water radiometry. *Appl. Opt.,* **44,** 553–567.

——, G. Lazin, G. Zibordi, and S. McClean, 2002a: An evaluation of above- and in-water methods for determining water-leaving radiances. *J. Atmos. Oceanic Technol.,* **19,** 486–515.

——, S. McLean, J. Sherman, M. Small, G. Lazin, G. Zibordi, and J. W. Brown, 2002b: The Seventh SeaWiFS Intercalibration Round-Robin Experiment (SIRREX-7), March 1999. NASA Tech. Memo. 2002–206892, Vol. 17, S. B. Hooker and E. R. Firestone, Eds., NASA Goddard Space Flight Center, 69 pp.

——, G. Zibordi, J.-F. Berthon, and J. W. Brown, 2004: Above-water radiometry in shallow coastal waters. *Appl. Opt.,* **43,** 4254–4268.

Jin, Z., T. Charlock, and K. Rutledge, 2002: Analysis of broadband solar radiation and albedo over the ocean surface at COVE. *J. Atmos. Oceanic Technol.,* **19,** 1585–1601.

Lerner, B., H. Guterman, M. Aladjem, and I. Dinstein, 1999: A comparative study of neural network based feature extraction paradigms. *Pattern Recognit. Lett.,* **20,** 7–14.

Loisel, H., and A. Morel, 2001: Non-isotrophy of the upward radiance field in typical coastal (Case 2) waters. *Int. J. Remote Sens.,* **22,** 275–295.

Magnuson, A., L. W. Harding, M. E. Mallonee, and J. E. Adolf, 2004: Bio-optical model for Chesapeake Bay and the Middle Atlantic Bight. *Estuarine Coastal Shelf Sci.,* **61,** 403–424.

Maritorena, S., A. Morel, and B. Gentili, 1994: Diffuse reflectance of oceanic shallow water: Influence of water depth and bottom albedo. *Limnol. Oceanogr.,* **39,** 1689–1703.

Mélin, F., G. Zibordi, and J.-F. Berthon, 2007a: Assessment of satellite ocean color products at a coastal site. *Remote Sens. Environ.,* **110,** 192–205.

——, ——, and S. Djavidnia, 2007b: Development and validation of a technique for merging satellite derived aerosol optical depth from SeaWiFS and MODIS. *Remote Sens. Environ.,* **108,** 436–450.

Mobley, C., 1999: Estimation of the remote-sensing reflectance from above surface measurements. *Appl. Opt.,* **38,** 7442–7455.

Moody, E. G., M. D. King, S. Platnick, C. B. Schaaf, and F. Gao, 2005: Spatially complete global spectral surface albedos: Value-added datasets derived from Terra MODIS land products. *IEEE Trans. Geosci. Remote Sens.,* **43,** 144–158.

Morel, A., D. Antoine, and B. Gentili, 2002: Bidirectional reflectance of oceanic waters: Accounting for Raman emission and varying particle scattering phase function. *Appl. Opt.,* **41,** 6289–6306.

Mueller, J. L., and R. W. Austin, 1995: Ocean optics protocols for SeaWiFS validations, revision 1. NASA Tech. Memo. 104566, Vol. 55, S. B. Hooker and E. R. Firestone, Eds., NASA Goddard Space Flight Center, 67 pp.

Park, Y.-J., and K. Ruddick, 2005: Model of remote-sensing reflectance including bidirectional effects for case 1 and case 2 waters. *Appl. Opt.,* **44,** 1236–1249.

Santer, R., and C. Schmechtig, 2000: Adjacency effects on water surfaces: Primary scattering approximation and sensitivity study. *Appl. Opt.,* **39,** 361–375.

Sei, A., 2007: Analysis of the adjacency effects for two Lambertian half-spaces. *Int. J. Remote Sens.,* **28,** 1873–1890.

Smirnov, A., B. N. Holben, T. F. Eck, O. Dubovik, and I. Slutsker, 2000: Cloud screening and quality control algorithms for the AERONET database. *Remote Sens. Environ.,* **73,** 337–349.

Sosik, H., R. Green, W. Pegau, and C. Roesler, 2001: Temporal and vertical variability in optical properties of New England shelf waters during late summer and spring. *J. Geophys. Res.,* **106** (C5), 9455–9472.

Subramaniam, A., and Coauthors, 1999: CSC Technical Report: NOAA CSC 99043-PUB. NOAA Cruise JUL98NAN: Nantucket Shoals Cruise, NOAA, 47 pp.

Walker, J. H., C. L. Cromer, and J. T. McLean, 1991: Technique for improving the calibration of large-area sphere sources. *Calibration of Passive Remote Observing Optical and Microwave Instrumentation,* B. W. Guenther, Ed., International Society for Optical Engineering, (SPIE Proceedings, Vol. 1493), 224–230.

Werdell, J. P., and S. W. Bailey, 2005: An improved in-situ bio-optical data set for ocean color algorithm development and satellite data product validation. *Remote Sens. Environ.,* **98,** 122–140.

Zibordi, G., and J. F. Berthon, 2001: In situ relationships between the Q-factor and seawater optical properties in coastal regions. *Limnol. Oceanogr.,* **46,** 1130–1140.

——, S. B. Hooker, J.-F. Berthon, and D. D'Alimonte, 2002: Autonomous above water radiance measurements from stable platforms. *J. Atmos. Oceanic Technol.,* **19,** 808–819.

——, F. Mélin, S. B. Hooker, D. D'Alimonte, and B. Holben, 2004: An autonomous above-water system for the validation of ocean color radiance data. *IEEE Trans. Geosci. Remote Sens.,* **42,** 401–415.

——, ——, and J.-F. Berthon, 2006a: Comparison of SeaWiFS, MODIS and MERIS radiometric products at a coastal site. *Geophys. Res. Lett.,* **33,** L06617, doi:10.1029/2006GL025778.

——, ——, and ——, 2006b: A time series of above-water radiometric measurements for coastal water monitoring and remote sensing product validation. *IEEE Geosci. Remote Sens. Lett.,* **3,** 120–124.

——, and Coauthors, 2006c: A network for standardized ocean color validation measurements. *Eos, Trans. Amer. Geophys. Union,* **87** (30), doi:10.1029/2006EO300001.

——, N. Strömbeck, F. Mélin, and J.-F. Berthon, 2006d: Tower-based radiometric observations at a coastal site in the Baltic Proper. *Estuarine Coastal Shelf Sci.,* **69,** 649–654.

——, J. F. Berthon, F. Mélin, D. D'Alimonte, and S. Kaitala, 2009: Validation of satellite ocean color primary products at optically complex coastal sites: Northern Adriatic Sea, northern Baltic Proper and Gulf of Finland. *Remote Sens. Environ.,* in press.